https://doi.org/10.1142/9789811280184_0026

Chapter 26

High Energy LHC Machine Options in the LHC Tunnel

Luca Bottura and Frank Zimmermann

CERN, Esplanade des Particules 1, 1217 Meyrin, Switzerland

The LHC infrastructure, i.e. the tunnel itself as well as the services associated with power, cooling, ventilation, network and access (among others), represent a considerable asset, and may be considered for hosting and supporting future versions of a "LHC" beyond its present configuration and the HL-LHC upgrade. In this chapter, we provide an overview of possible machine parameters and energy reach of a future higher-energy hadron collider in the LHC tunnel. We sketch four options with arc dipole magnetic fields in the range of 12 T to 24 T, each of which represents a well-defined discrete step in future accelerator magnet technology. We discuss the corresponding main machine and magnet parameters, and describe readiness, challenges and opportunities.

Keywords: High Energy LHC; Nb_3Sn accelerator dipoles; HTS accelerator dipoles

1. Introduction

The LHC has a considerable value, which is customarily associated with the existing and running accelerator and experiments. Also, the site infrastructure in itself, extending from civil engineering to powering, cooling, ventilation and other auxiliary systems, is a noticeable asset. Hence, it is natural that several past analyses and studies discussed the possibility of using the LHC site infrastructure for upgrades well beyond the lifetime of the LHC and the HL-LHC.

The 2002 Feasibility Study for an LHC Luminosity and Energy Upgrade[1] defined an "LHC Phase 2", which consisted of installing new superconducting dipoles in the LHC arcs to reach a beam energy around

12.5 TeV. The Study Report pointed out that "the energy upgrade is much easier to exploit than a luminosity upgrade, as it requires minimal changes to the detectors. Dipole magnets with a nominal field of 15 T and a safety margin of about 2 T can be considered a reasonable target...".

This idea was followed up in 2010, when a High-Energy LHC (HE-LHC) based on 20 T hybrid magnets was studied by a dedicated working group. This activity culminated in the HE-LHC'10 EuCARD workshop.[2] The HE-LHC'10 workshop also, for the first time, proposed a future Very High Energy LHC (VHE-LHC), a new ring with a larger ~ 80 km circumference, which later became the Future Circular Collider hadron-hadron option (FCC-hh).[3]

The FCC-hh study took the proposal of the VHE-LHC further, developing a full design for a hadron collider with a tunnel length in the range of 80 to 100 km. An annex activity to FCC-hh was to study an energy upgrade in the LHC tunnel made possible by the magnet technology to be developed for the FCC-hh. The HE-LHC, based on the 16 T magnets of the FCC-hh case, including dispersion suppressor (DS), Interaction Regions (IRs), and collimations, is described in detail in the FCC design report volume 4.[4] This option was shown to require a new superconducting SPS (sc SPS) as injector to reach acceptable injection field and aperture.

Finally, a recent study considered the possibility of a partial energy increase of the present LHC that could be obtained by using the HL-LHC 11 T dipoles to replace one third of the present Nb-Ti dipoles by higher field Nb_3Sn magnets.[5] This would result in a modest increase in energy reach, i.e. a centre-of-mass (COM) energy of 16.2 TeV vs. 14 TeV nominal for the LHC, and was not retained as an interesting investment by the authors of the study. Still, it is instructive to consider what would be the result of using the magnet technology under development for the ongoing HL-LHC upgrade, just short of 12 T, as a full replacement for the present LHC.

Taking into account the historical proposals and studies, we have selected four scenarios that could represent well-defined discrete and distinct options for a future High-Energy (HE) hadron collider in the LHC tunnel, following the completion of the HL-LHC physics programme, namely:

- A modest energy upgrade based on technology close to deployment, i.e., Nb_3Sn 12 T dipoles, leading to a COM energy of 20 TeV. We refer to this option as HE20.
- The highest energy that could be reached by Low Temperature Superconductor (LTS) accelerator magnet technology, i.e., the

Nb_3Sn 16 T dipoles being developed for the FCC-hh. In this case the COM energy would be about 27 TeV, and we denote this option by HE27.

- Higher dipole fields as could be reached if High Temperature Superconductor (HTS) dipole magnets can be developed as outlined in the HE-LHC proposal, namely 20 T, leading to a COM energy of 34 TeV. This option is called HE34.
- Finally, we consider an ultimate High Energy LHC, namely taking HTS magnets producing a dipole field of 24 T, which possibly is the highest field range that can be reached with such technology. The reason for setting this bound is that forces, stored energy and cost will be about one order of magnitude larger than for the LHC magnets, requiring extraordinary advances in material science and engineering. This option, with name HE41, would yield a COM energy of 41 TeV.

In the following sections, we will elaborate on the collider parameters for the four options, and discuss the dipole magnet designs that would correspond to such parameters. For the relevant magnet technology, we base the discussion on ongoing developments, while referring to the designs proposed in the past, but we also elaborate on a perspective where we consider advances and activities in other fields of application of superconducting magnet technology.

2. Main Collider Parameters

The options outlined in the previous section are detailed in Table 1, which compiles the main machine and magnet parameters. The figures reported there are a combination of results from the references quoted earlier, and scaling applied to such options. Note that for the discussion we only report the required dipole field, expanding, in a later section, on the possible magnet configurations and challenges. It is clear that a complete analysis of any option would require devising quadrupoles and dispersion suppressor magnets, as well as adapted insertions. Indeed, simple scaling from LHC and HL-LHC does not necessarily produce consistent and feasible configurations, as the optics for the different energy options may differ considerably. This point is illustrated by the study of the HE-LHC based on FCC-hh 16 T dipoles.[4] A detailed discussion on how the optics is modified by using different dipole configurations and strength can also be found in Ref. 6.

Still, in spite of the simple approach taken here, our basic considerations suffice to provide a good view of the perspective and challenges of an HE-LHC.

Table 1. Key parameters of four HE-LHC options compared with HL-LHC and LHC, for operation with proton beams. All values, except for the injection energy itself, refer to the collision energy. The ring circumference is 26.7 km and the straight section length 528 m, as for the existing LHC tunnel.

Parameter	Unit	HE20	HE27	HE34	HE41	(HL-)LHC
Centre-of-mass energy	TeV	20	27	34	41	14
Injection energy	TeV	0.6	0.8	1.0	1.2	0.45
Peak arc dipole field	T	12	16	20	24	8.33
Beam current	A	1.12				(1.12) 0.58
Bunch population	10^{11}	2.2				(2.2) 1.15
Bunches / beam		2808				(2760) 2808
Rf voltage	MV	16				(16) 16
Rf frequency	MHz	400				(400) 400
momentum compaction	10^{-4}	5.8				(3.22) 3.22
RMS bunch length	mm	~ 90				(90) 75.5
Bucket half height	10^{-3}	0.24	0.21	0.19	0.18	0.36
RMS momentum spread	10^{-4}	0.77	0.67	0.59	0.54	1.129
Longit. emit. ($4\pi\sigma_z\sigma_E$)	eVs	2.9	3.3	3.7	4.0	2.5
Bunch spacing	ns	25				25
Norm. tr. rms emittance	µm	2.5				(2.5) 3.75
IP beta function $\beta^*_{x,y}$	m	0.25	0.45	0.55	0.60	(0.15) 0.55
Initial IP beam size $\sigma^*_{x,y}$	µm	7.7	8.8	8.7	8.3	(7.1 min.) 16.7
Half crossing angle	µrad	160	104	84	74	(250) 142.5
Initial luminosity / IP	$\mathrm{nb}^{-1}\mathrm{s}^{-1}$	200	160	160	180	(50, levelled) 10
Total cross section	mbarn	119	126	131	135	111
Inelastic cross section	mbarn	87	91	94	97	85
Initial events / crossing		570	450	480	540	(135) 27
RMS luminous region	mm	~ 64				(64) 45
Stored energy / beam	GJ	1.0	1.3	1.7	2.0	(0.7) 0.36
Energy loss / p / turn	keV	28	93	230	470	6.7
SR power / beam	kW	30	100	251	532	(7.3) 3.6
SR power / length	W/m/ap.	1.4	4.6	11.5	24.5	(0.33) 0.17
Transv. emit. damp. time	h	8.8	3.6	1.8	1.0	25.8
No. of high-luminosity IPs	—	2				(2) 2
Initial proton burn-off time	h	3.5	4.4	4.1	3.6	(15) 40
Allocated physics time / yr	days	160	160	160	160	160 (160)
Average turnaround time	h	5				4 (5)
Optimum run time	h	4.5	5.2	4.7	4.3	(18–13) ∼10
Accelerator availability	—	75%				(80%) 78%
Ideal luminosity / day	fb^{-1}	4.1	4.2	4.3	4.4	(1.9) 0.4
Luminosity per year	fb^{-1}	490	500	520	530	(240) 55

In Table 1, the centre-of-mass collision energy increases in proportion to the arc dipole field. Higher injection energy, attainable from a new superconducting (sc) SPS, is required for adequate dynamic and physical aperture.

In case of Nb_3Sn magnets, the field quality at injection can be improved by a superconductor with reduced low-field magnetization,[4] which would provide a solution for low-field injection. However, compared with the present LHC, at higher energy a more voluminous beam screen is required to intercept the synchrotron-radiation (SR) photons and to extract the increasing SR heat load, while still ensuring a good vacuum quality together with a low machine impedance. Consequently, the actual physical half aperture available for the injected beam shrinks from about 2 cm for the LHC to 1.3 cm for the HE-LHC.[4] Following Ref. 4, in view of the more challenging physical and dynamic aperture constraints, we assume that the injection energy needs to increase roughly in proportion to the collision energy.

For all scenarios we consider the same beam current I_b, bunch population N_b, transverse normalized emittance ε_n, and rms bunch length σ_z as for the HL-LHC. These beam parameters are available from the LHC injector complex after its recent upgrade (LIU).[7]

In Ref. 4, two optics were studied. For the scenarios HE20 to HE41, we assume the optics with 18 FODO cells per arc and a FODO cell length of 137.33 m instead of 23 FODO cells with a cell length of 106.9 m, as for the LHC and HL-LHC, one advantage being a 5% higher energy reach at the same dipole field. For this optics, the momentum compaction factor α_C is more than doubled compared with the LHC. The bucket height scales as $\sqrt{V_{\mathrm{RF}}/(E_b\alpha_C)}$. Keeping the rf voltage constant, equal to 16 MV, for a given optics, the bucket height scales as the inverse square root of beam energy. In Table 1, we scale the rms energy spread in proportion to the bucket height, which makes the rms relative energy spread decrease as the inverse square root of the beam energy, and the longitudinal emittance rise as the square root of the beam energy E_b. This scaling also ensures longitudinal Landau damping.[8,9]

It is natural to assume high-luminosity collisions in $n_{\mathrm{IP}} = 2$ primary collision points, and possible lower-luminosity secondary collisions at two other IPs, as for the LHC and HL-LHC. We take the total number of bunches n_b to be 2808, as was in the original LHC design, slightly larger than the 2760 value of the HL-LHC.[10] Higher beam energies will, however, require a revision of the dump and injection kicker system, which may have an impact on the maximum number of bunches permitted.

The HE-LHC optics design of Ref. 4 for a centre-of-mass energy of 27 TeV achieved an interaction point (IP) beta function β^* of 0.45 m, with acceptable dynamic aperture. We assume the same value for HE27, recognizing that HL-LHC aims for 0.15 m, and interpolate between these values, as well as extrapolating for higher energies. This results in a roughly constant rms interaction-point (IP) beam size between 8 and 9 μm for all energies.

To maintain a constant impact of long-range collisions on the beam lifetime, the crossing angle θ_c scales as $\theta_c \propto 1/\sqrt{\beta^* E_b}$, that is in proportion to the IP beam divergence. In Table 1 we are assuming that the triplet length and the total number of long-range collisions stays approximately the same as for the HL-LHC. We note that for the 16 T HE27 scenario this scaling leads to a full crossing angle of 208 mrad, as indicated, whereas for the longer HE-LHC triplet considered in Ref. 4, and for the same IP beta function $\beta^*_{x,y} = 0.45$ m, a much larger crossing angle of 330 mrad was chosen. As for the HL-LHC and the HE-LHC of Ref. 4, crab cavities will be needed to avoid luminosity loss due to the crossing angle.

The initial luminosity is given by

$$L_0 = \frac{f_{\rm rev} n_b N_b^2}{4\pi {\sigma^*_{x,y}}^2} \ , \tag{1}$$

where $f_{\rm rev}$ denotes the revolution frequency, and $\sigma^*_{x,y} = \sqrt{\beta^* \varepsilon_n/\gamma}$ the rms beam size at the IP, assuming round beams ($\sigma^*_y = \sigma^*_x$), and $\gamma = E_b/(m_p c^2)$ the relativistic Lorentz factor, with m_p the proton mass and c the speed of light.

The total and inelastic proton-proton cross sections, $\sigma_{\rm tot}$ and $\sigma_{\rm inel}$, are weakly dependent on the collision energy as indicated. This dependence is described by Eqs. (6) and (7) in Ref. 11, which are based on Refs. 12–17. The total cross section $\sigma_{\rm tot}$ increases from about 111 mbarn at 14 TeV (LHC) to 135 mbarn at 41 TeV centre-of-mass energy (HE41), the inelastic cross section $\sigma_{\rm inel}$ from 85 to 97 mbarn. The inelastic cross section roughly relates to the number of events per bunch crossing recorded in the detector (the so called event pile up), as

$$n_{\rm event} = \frac{\sigma_{\rm inel} L_0}{n_b f_{\rm rev}} \ . \tag{2}$$

The initial pile up is about 500 per bunch crossing for all four HE-LHC versions considered. Especially for HE34 and HE41 the pile up will increase during the physics store. With perfect crab crossing and for Gaussian bunch

profiles, the rms extent of the luminous region is equal to the rms bunch length divided by $\sqrt{2}$.

The total cross section $\sigma_{\rm tot}$ determines the initial proton burn off time $\tau_{\rm bu}$ as

$$\frac{1}{\tau_{\rm bu}} = -\frac{\dot{N}_b}{N_b} = \frac{\sigma_{\rm tot} L_0 n_{\rm IP}}{N_b n_b} \ . \tag{3}$$

The energy stored in the beam scales exactly with beam energy, and at highest beam energy (HE41) approaches a value of 2 GJ, which is about 3 times higher than for the HL-LHC.

The proton energy loss per turn due to synchrotron radiation grows as the fourth power of beam energy, increasing from 6.7 keV at the LHC to 470 keV at HE41. At constant beam current and bending radius, the total synchrotron-radiaton power also increases as the fourth power of energy. While for the nominal LHC, the SR power of one beam is 3.6 kW, for the HE41 it becomes 500 kW per beam, or about 1 MW in total, and the synchrotron radiation per unit length reaches 25 W/m per aperture, which is almost the same as the 29 W/m per aperture of the FCC-hh design. This implies that the SR heat can still be removed from inside the arcs with the FCC-hh/HE-LHC beam screen design. At even higher energies, the maximum allowable synchrotron radiation heat load would limit the maximum beam current.

The radiation damping time scales as ρE_b^{-3}, where ρ denotes the dipole bending radius. The interplay of proton burn off and radiation damping determines the optimum physics run time (i.e. the moment the two beams are dumped for a new injection) as a function of the average turnaround time (the time between the dump and the start of the new physics fill).

If the proton burn-off time is shorter than the transverse emittance damping time, as is the case for HE20, the beam-beam tune shift decreases during the store, and the calculation of the optimum run time $t_{\rm r}$ is based on Eqs. (2.2)–(2.4) of Ref. 4. In the opposite the case, both the luminosity and the beam-beam tune shift increase with time in store, and for the latter we must assume a maximum acceptable value, which, once reached, is maintained by controlled emittance blow up through transverse noise excitation, as is proposed for the FCC-hh.[11] The time evolutions of the luminosity and the optimum run length $t_{\rm r}$ then follow from Eqs. (33)–(54) in Ref. 11. This situation is encountered for HE27, HE34 and HE41. For the purpose of illustration, we consider a maximum beam-beam tune shift of 0.025, which is close to the value of 0.03 assumed for the "phase 2" of the FCC-hh.[3,11] The ideal evolution of instantaneous and integrated luminosity

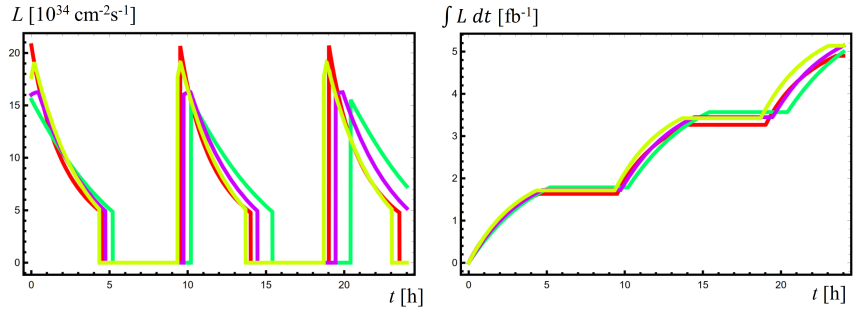

Fig. 1. Instantaneous (left) and integrated luminosity (right) as a function of time during 24 hours with 25 ns bunch spacing, for HE-LHC options HE20 (red), HE27 (green), HE34 (purple), and HE41 (yellow); considering a maximum total beam-beam tune shift of 0.025.

during 24 h is shown in Fig. 1, for all four HE-LHC versions. The increase of the instantaneous luminosity during the early store for HE34 and HE41 also is a measure of the increase of the event pile up from its initial value, which is of order 10%.

For the average turnaround time and for the number of physics days per year, we adopt the canonical values of Ref. 18 (5 hours and 160 days). The ideal integrated luminosity per day is then computed for the optimum run time t_r and the assumed average turnaround time. The luminosity delivered per year is finally obtained by multiplying the latter with the number of physics days scheduled and the postulated availability of 75%,[18] which is slightly lower than for the LHC and HL-LHC.

3. Dipole Magnets for a LHC Energy Upgrade

The technology driver of the magnet system of a collider are the main bending dipoles, determining the maximum energy that can be reached, and representing, by far, the most expensive item. In general, the dipole magnets also represent the main challenges in the whole magnet system well, including the arc and final focus quadrupoles. Our discussion revolves around dipole concepts suitable for the collider options outlined in Table 1. We are aware that this is only a partial picture of the whole magnet system, though appropriate for our scope.

The idea of developing new dipoles for an energy upgrade of the LHC has gone hand in hand with the considerations of new machine configurations described in the introduction. Several magnet concepts and designs for a

high energy LHC have been considered and presented in the past thirty years, starting even before the LHC construction was completed.

One of such works first documented is Ref. 19, proposing, in 2005, a 24 T dipole magnet for an energy tripler solution, fitting the requirements for the HE41 option described above. At the 2010 HE-LHC workshop[20] a somewhat more modest field was considered; a dipole magnet generating 20 T.[21,22] This dipole magnet corresponds to the HE34 option reported in Table 1. More recently, as a part of the Future Circular Collider study, 16 T magnet designs were derived from the FCC-hh and adapted for installation in the LHC tunnel.[23] The adapted FCC dipoles are those that yield a collider with the characteristics of the HE27 option. Finally, the present HL-LHC construction work[24] is producing dipoles and quadrupoles with ultimate and peak fields in the range of 12 T,[25,26] i.e. the field required for the HE20 collider option of Table 1.

Below, we describe the designs from the quoted references, including some adjustments when necessary, paying special attention to available technology, or expected advances from on-going R&D. We will not go into details of the designs, but rather, we will concentrate on field goals, broad design choices and other prime characteristics such as electromechanical forces and stored energy density, including considerations on the planned and necessary developments to achieve such goals. We will then summarize the main results and discuss alternative approaches that could be of interest in the long term.

Table 2 presents a summary of the main parameters and characteristics of the designs referenced, including field, current, selected operating temperature, coil dimensions, cold mass and cryostat diameter, structural support concept, total forces (acting on a quarter of the dipole coil), stored energy, and energy density. The values of horizontal force and energy density are also plotted in Figs. 2 and 3, together with analogous values of collider and development dipole magnets. This is useful, putting the selected dipole designs in the perspective of past realizations and on-going developments. In fact, Figs. 2 and 3 are a good representation for the main challenges of high field dipoles, namely mechanical stresses and quench protection under increased electromagnetic loads and stored magnetic energy.

In Table 2, we also include a Technology Readiness Level (TRL) indicator, and a relative cost indicator. The TRL provides a standard measurement of the maturity of a technology, ranging from the lowest readiness level 1 (basic principle demonstration) to the highest readiness level 9 (proven technology in application). The cost indicator is given by referring

Table 2. Summary of main design parameters, characteristics, and performance indicators for the four dipole designs described here.

Parameter	Unit	HE20	HE27	HE34	HE41
Dipole field	T	12	16	20	24
Operating current	kA	16	22	N/A	33
Operating temperature	K	1.9	1.9	1.9	4.2
Superconducting material	—	Nb_3Sn	Nb_3Sn	Nb_3Sn	Nb3Sn
				REBCO	Bi-2212
Supporting structure concept	—	Collars	Bladder-and-key		
Aperture	mm	50	50	40	40
Operating current density	A/mm^2	480	480	380	580
Coil cross section (one aperture)	mm^2	6500	10000	18000	12500
LTS cross section	mm^2	6500	10000	12500	6100
HTS cross section	mm^2	0	0	5500	6400
Cold mass outer diameter	mm	570	8600	800	750
Cryostat outer diameter	mm	914	1200	>1200	1200
Horizontal force	kN/m	2727	5470	10063	12149
Vertical force	kN/m	2270	4335	7287	9041
Stored energy	kJ/m	522	1171	2448	2578
Stored energy density	J/cm^3	80	115	136	270
TRL	—	4	3	2	2
Cost at present	a.u.	1.2	1.6	5	13
Cost perspective	a.u.	0.5	0.7	1.5	5

to the cost of the Nb_3Sn magnets for HL-LHC, taken equal to one. For this evaluation we have removed the cost of R&D, tooling and infrastructure, as well as fringe costs related to the small-scale HL-LHC production. The resulting cost per m of magnet is in the range of 400 kCHF/m, which is consistent with the projection of using 11 T dipoles for a partial energy upgrade of the existing LHC.[5] Two assumptions were made to evaluate the relative cost indicator. The first assumption is based on superconductor costs per unit weight as they currently are, where the cost of REBCO per unit mass is about four times that of Nb_3Sn, while the cost of Bi-2212 is about twelve times higher. The corresponding values have been indicated as "*present*" relative cost indicator. The second assumption is based on a cost reduction that could result from on-going developments and a perspective production scale up.

For Nb_3Sn the targeted reduction is a factor of three,[27] in which case the cost per kg would be comparable to that of the ITER production. This would correspond to a superconductor cost equal to three times the cost of raw material, i.e. a factor P = 3, as discussed in Ref. 28 where P is defined as the ratio of conductor to raw material cost. The cost reduction assumed

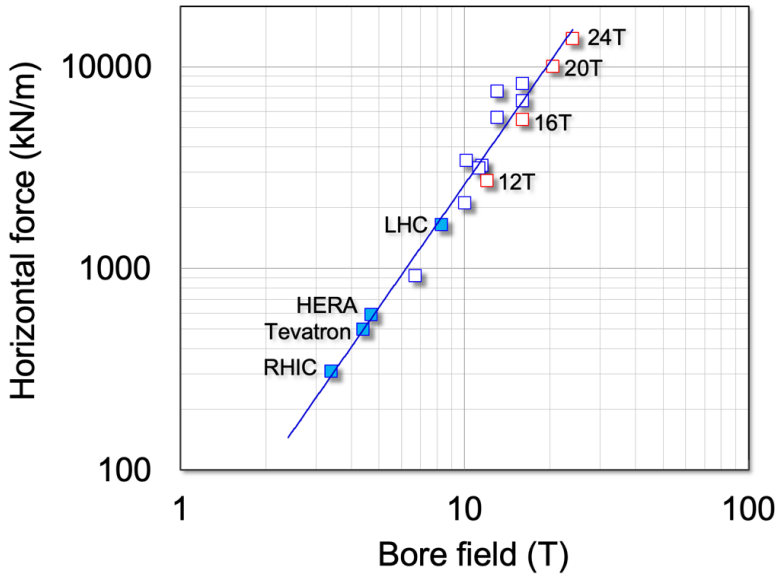

Fig. 2. Scaling of horizontal electromagnetic force per unit length (one coil quarter) vs. magnetic field. The scatter plot reports values for built colliders (blue, solid), magnet models and designs (blue, empty), and the four dipole designs described here (red empty).

for REBCO is a factor four, which would yield a cost per unit weight equal to the present Nb_3Sn for HL-LHC. This would still correspond to a P factor of several hundreds, recognizing the higher process complexity of REBCO manufacturing. At the same time, such a high P factor points to a remarkable potential for cost reduction in case capacity is further scaled up, and the process simplified. For Bi-2212 the cost reduction assumed is a factor 2.5, and a resulting cost five times that of present Nb_3Sn for HL-LHC. This is justified by the fact that the cost of Ag is one order of magnitude higher than that of Cu. As a result, in the case of Bi-2212, the projected cost reduction would correspond to a factor $P = 10$, i.e. comparable to that of present Nb_3Sn. This also shows, contrary to REBCO, that there is not much room for a further substantial reduction in this case. The resulting costs with these assumptions have been identified as "*perspective*".

3.1. *12 T dipole*

The first, more modest, energy upgrade version of Table 1, HE20, requires collider dipoles operating at 12 T. This field is beyond the reach of Nb-Ti,

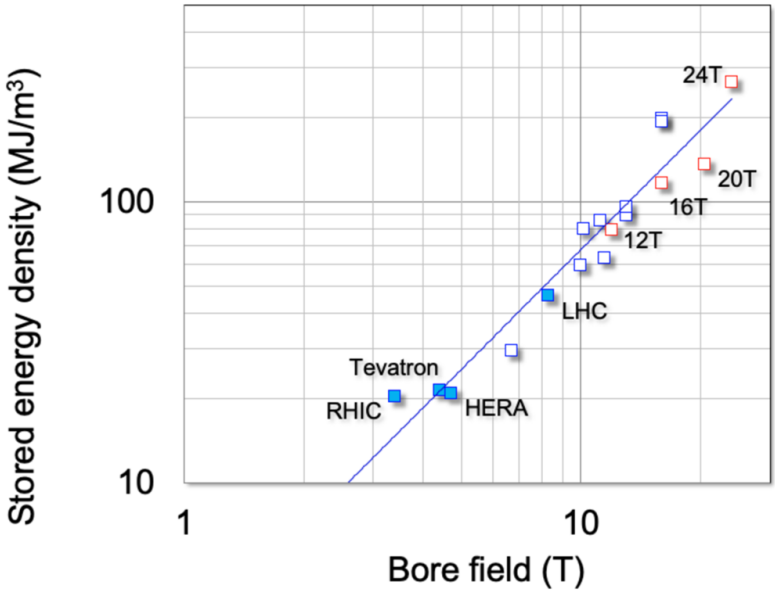

Fig. 3. Scaling of stored magnetic energy density per unit volume vs. magnetic field. The scatter plot reports values for built colliders (blue, solid), magnet models and designs (blue, empty), and the four dipole designs described here (red empty).

the well established accelerator magnet technology for all past and present colliders. A bore field of 12 T can be reached using Nb_3Sn using existing wires and cables, as demonstrated by the results achieved with the 11 T short models and long magnets.[25,26] For this reason we take the 11 T dipole as a good basis for extrapolation.

The HL-LHC 11 T development, initially launched as a collaboration between CERN and FNAL,[29] is presently on-going within the scope of HL-LHC. A cross section of the 11 T magnet is shown in Fig. 4, showing the cos-theta coils, enclosed and supported by a collared coil structure, and the twin aperture assembly in a single iron yoke. The main design and manufacturing features of this magnet, and the results achieved by the development program, can be found in Ref. 26.

The 11 T dipole was designed for compatibility with the existing LHC magnets. This imposed a number of strong constraints on several aspects. The geometry, including length, outer diameter, and inter-beam distance, were fixed to fit with the envelope of a LHC main dipole. The operating current and corresponding magnetic field resulted from the need to be

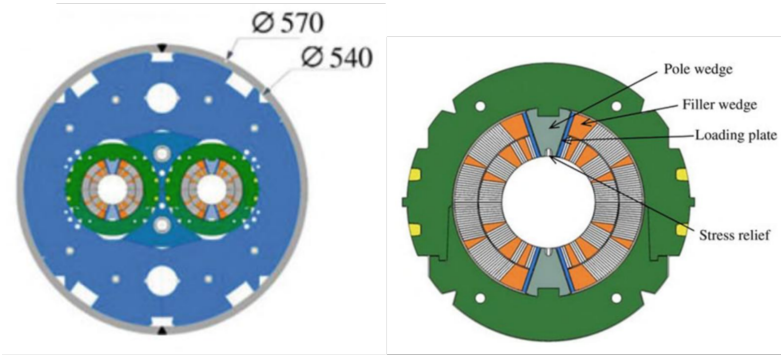

Fig. 4. Cross section of the HL-LHC 11T twin aperture dipole, showing the twin aperture cold mass (left), and the collared coil (right), reproduced from Ref. 26.

powered in series with the LHC main dipole circuit. For the same reason the 11 T dipoles were designed to operate in superfluid helium, at 1.9 K, as the rest of the LHC arc. The operating point resulting from the challenging design optimization was set at 80% of critical conditions along the magnet load line. This corresponds to a fraction of critical current of about 50%, and a temperature margin of at least 4.5 K. The 11 T dipoles are built as straight magnets of 5.31 m magnetic length. The coil aperture, 60 mm, larger than that of the LHC main dipoles, allows for a comfortable space for the beam sagitta. Finally, given the limited number of magnets to be installed (2 units consisting of 2 magnets each, compared to 1230 main dipoles in the rest of the LHC), the specification on the field quality could be relaxed. The persistent current contribution to the normal sextupole is of the order of 40 units, with a variation by more 10 units during the ramp, an order of magnitude larger than in the LHC. While this was found to be acceptable from the point of view of beam performance in the LHC, it will surely need to be reduced for a collider based on this magnet type, also because of AC loss, i.e. the energy dissipation associated with the change of magnetization.

Three out of four 11 T series magnets, units fully equipped for installation in the LHC, achieved the nominal current at the first thermal cycle, and sustained repeated simulated ramps, demonstrating that this field level is within reach with an adequate operating margin.[30] Further tests have shown, however, that performance retention through powering and thermal cycles is an issue. Degradation and some erratic quenches were observed in these full-size magnets, likely related to localized breakage of

the brittle Nb_3Sn superconducting filaments. R&D is actively pursued to identify causes and mitigate this effect, which is presently attributed to coil stress and strain concentration, possibly already at the stage of construction, followed by variations of such state during the magnet lifetime. In fact, concerns on stress peaks were already identified earlier in the 11 T program, and mitigated by intentionally reducing the amount of coil pre-compression applied during collaring. It was found that the coil pre-stress could be reduced below the value required to guarantee that the coil remains compressed against the collar pole at full current, and yet the magnet still reaches nominal field. This suggests that full pre-stress may not be necessary for the impregnated and stiff Nb_3Sn coils, a major change in the design paradigm for collared, cos-theta coils.

In the perspective of a new accelerator realization, the constraints on coil and magnet characteristics can be relaxed to a certain degree. This would allow for a reduction of stress and stored energy density, both of which would be beneficial to resolving the concern of robustness of the present 11 T, and easing magnet protection from quench. This evolution is in fact one of the two main avenues pursued by the R&D Programme on High Field Nb_3Sn accelerator Magnets (HFM),[31] that seeks to demonstrate that Nb_3Sn technology is fit for deployment on large scale.

A modification of the 11 T design to produce a 12 T dipole is outlined in Table 2, where we report approximate coil dimensions, field and current, and structure selection. A suitable cable option could be a scaled-up version of the 11 T cable, going from a 0.7 mm strand to a 0.85 mm strand, and a 40 strands cable, identical to that used for the HL-LHC interaction region quadrupoles (QXF).[32] The coil width increases by approximately 20%, and we maintain the same operating margin, which has been shown to result in limited training to operating conditions, enough for operation. To achieve this margin, the cable current density is reduced by about 10% with respect to the 11 T dipole.

The operating temperature of this dipole is set to 1.9 K, as in the LHC. The main reason is to profit from the good heat transfer properties of stagnant superfluid helium acting as thermal vector for the cold mass. Unlike Nb-Ti, the additional operating margin of Nb_3Sn at 1.9 K with respect to liquid helium conditions, 4.2 K, would not, by itself, justify the additional cooling effort for a 12 T dipole. This is also true because heat transfer from an impregnated coil, the standard for Nb_3Sn, is rather governed by heat conduction than by heat transfer to the helium bath. Alternatives to a pool bath of helium could hence be devised to reduce the helium inventory of a 12 T dipole.

For the modest field increase to 12 T we can still assume that collars provide a suitable structural support, under the assumption that pre-loading of the coil is limited to the maximum acceptable conductor transverse stress, with large margin (e.g. setting a maximum in the range of 100 MPa on the coil midplane). The cold mass diameter can be maintained at the standard of the LHC dipole, 570 mm, as was done for the 11 T dipole, at the expense of some field leakage and marginally degraded field quality at high field. These effects should be minor and manageable. The result is an outer cryostat diameter identical to that of the present LHC, which can be integrated into the existing tunnel infrastructure.

The increased conductor width partially compensates for the increase in forces and results in lower accumulated electromagnetic stress on the midplane, by about 10%. Lower pre-stress and electromagnetic stress allow increased robustness to geometric errors, assembly tolerances and local stress intensification factors. These choices all lead to easier manufacturing and, in the end, cheaper magnets. Note, however, that despite the increased structural margin, significant development is still necessary to simplify manufacturing steps and tooling, reduce manipulation, reducing conductor cost.

It is for this reason that we assign a TRL of 4 to this dipole option in Table 2 (*technology validated in lab*). As for the relative cost, in present conditions this 12 T dipole would cost 1.2 times the reference HL-LHC cost. Provided that the Nb_3Sn R&D is successful in achieving its cost reduction targets,[27] we can expect that the 12 T dipole option described here to be 0.5 times the reference HL-LHC cost. A relatively high TRL and moderate relative cost can be maintained as the main result of this dipole design, to be balanced by the modest reach of a HE20 collider.

3.2. *16 T dipole*

The second energy upgrade version, HE27, requires collider dipoles operating at 16 T, also built with Nb_3Sn. This is the field level targeted by the Future Circular Collider, and the design of this option is described in detail in Ref. 4. For the FCC-hh a cos-theta baseline is assumed, built with four layers, with graded cables, and assembled in a bladder and key structure. In fact, as mentioned in Ref. 4, several alternatives are possible, also detailed in Ref. 33, and it is not yet clear which conductor, coil and structure configuration is the optimal choice for this field level. Indeed, reaching this operating field level in a model accelerator dipole magnet has not yet been

demonstrated, although tests on conductors and racetrack coils, assembled in block coil configuration, have shown that it is possible to generate such fields with Nb_3Sn.[34,35]

Given the good performance of the block coil demonstrators, we take, for our discussion, the configuration shown in Fig. 5 as a suitable option of a 16 T dipole built with Nb_3Sn. Block coils are built as double pancakes with flared ends, stacked around the desired aperture. A description of the general features of block magnets and typical geometries can be found in Refs. 36–38. The main advantage of the block coil configuration is that it decouples the location of peak field, usually close to the inner coil perimeter, from the location of maximum stress, which in the case of block coils tends to be towards the outside perimeter, where the electro-magnetic force accumulates. Another interesting feature of block coils, important to the design and manufacturing of magnets in this field range, is that the coils can be made larger by simply winding more turns. The additional ampere-turns increase the operating margin, while a wider coil reduces the stress. This is not the case for a cos-theta coil, whose thickness is locked once the cable width is selected. The downside of block coils is that for maximum field efficiency the cable width must fit the given magnet aperture, which in our case results in large cables (ideally 25 mm cable width for a 50 mm aperture). This is however not a serious issue, given that large cables within this range have already been manufactured and tested within the scope of the ongoing efforts towards high field Nb_3Sn magnets.[37]

The configuration shown in Fig. 5 is an evolution of the program that has led CERN to the successful demonstration of 16.5 T peak field in racetrack

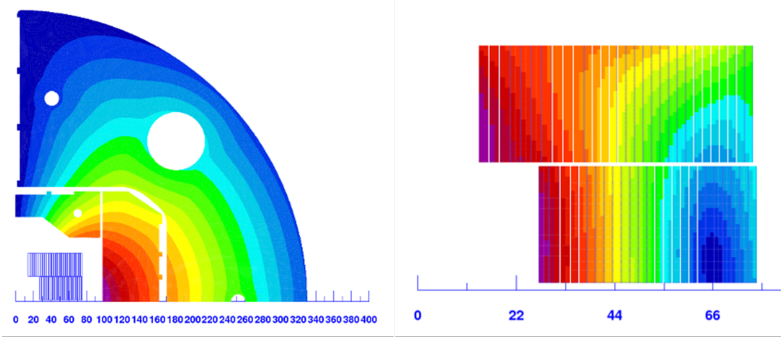

Fig. 5. Cross section of the 16 T block dipole designed as a demonstrator for FCC, a quarter of the whole magnet (left) and detail of the graded coil (right).[41]

coils quoted earlier (eRMC and RMM),[35] as well as the construction of the 14.6 T, 100 mm bore dipole for the FRESCA2 test facility, designed and built as a collaboration between CERN and CEA.[38] Conductors of characteristics required are being developed for the construction of the US Test Facility Dipole (TFD) at LBNL,[39] which should be used in the High Field Vertical Magnet Test Facility at FNAL to test future LTS and HTS cables.[40]

The operating temperature of this dipole is chosen at 1.9 K, as for the 12 T option. Besides the good heat transfer properties of a stagnant bath of superfluid helium permeating the cold mass already discussed, a 16 T field is at the upper bound within the reach of Nb_3Sn (in dipole magnets). In this case it is hence mandatory to aim for the lowest practical operating temperature to increase the operating margin, and keep the coil cross section as compact as possible.

The design consists of two pancake coils with flared ends, graded to reduce the coil cross section. The structure best adapted for this magnet and field level is based on the bladder-and-key principle. This system provides a pre-load that increases as the magnet cools down, owing to the differential of thermal contraction between the Al-alloy outer magnet shell and the internal magnet structure built of iron and steel. This is opposite to the collaring used in present accelerator magnets that tends to lose the pre-load as the magnet cools down. Bladder-and-keys have a large range of tuneability and allow the desired stress state to be reached gradually, without the need to over-stressing the coil during magnet assembly. Alternative systems have been proposed, all based on the same concept of exploiting differential thermal contraction.

Comparing the main magnet characteristics in Table 2, the 16 T dipole has significantly larger coil than the 12 T dipole — to compensate for the reduced critical current. The large coil helps to maintain both mechanical stress and stored energy density at reasonable level. The larger structure compared to the 12 T dipole, and the need to return a substantially larger magnetic flux, result in a larger cold mass diameter, 800 mm. This in turn requires an increase of the cryostat dimension, reaching values in the range of 1200 mm which is considered to be the largest diameter that can be integrated in the present LHC tunnel.

At this point, we need to note that the development towards a dipole of this level of field is substantial. As hinted above, demonstrations have, so far, been successful, but much work is required to improve conductor performance (to reduce magnet cost), engineer the magnet ends (still a

limitation in block coils), demonstrate effective conductor grading (required to make compact coils), and in general to make an accelerator magnet out of this promising concept (protection, field quality, alignment, heat transfer and cooling). For this reason a modest value of 3 is assigned to the TRL indicator (experimental proof of concept). Based on present conditions the relative cost indicator for this magnet is 1.6 times the HL-LHC reference. Assuming the Nb_3Sn superconductor cost reduction of a factor 3, the cost indicator would decrease to 0.7 of the present HL-LHC reference. This is substantial, but would still result in a magnetic system more than twice as expensive as the LHC — a relatively high price tag for a factor two increase in beam energy.

3.3. *20 T dipole*

Dipole fields in excess of 16 T, as required for the HE33 collider option, are well beyond the projected reach of LTS materials, and need a switch to HTS. Ideas on how to build a 20 T dipole were presented at the 2010 HE-LHC workshop in Malta,[20,21] and reviewed a few years later, together with other high field magnet options.[22] The basic idea of the design developed there is to profit from the HTS ability to generate high fields, but limit the amount of HTS material, still significantly more expensive than LTS. LTS can be used to generate a large portion of the field, grading the coil with different materials rather than different cable dimensions. This is akin to what done in high field solenoid magnets, where a small high field insert made in HTS is installed in a large bore outer magnet made of LTS. No specific HTS material was selected for the conceptual magnet design in Ref. 21, though at the time it seemed that Bi-2212, in round isotropic wires, could be a suitable choice. Several geometries and grading were considered in the following work.[22] We show in Fig. 6 the simplest among the options considered, with only two material grades, HTS and Nb_3Sn. This configuration is not the most efficient among all those studied, but retains a level of simplicity that is interesting from the point of view of manufacturing and cost reduction. An interesting consideration in Ref. 22 is the fact that field quality for any very high field dipole is not an issue, given that the coil cross section is forcibly large and the coil tends to naturally generate a good dipole field.

The main parameters of this magnet design are reported in Table 2. We note the expected increase of forces and stored energy per unit length, a factor about 4 with respect to the 12 T dipole described earlier. The design

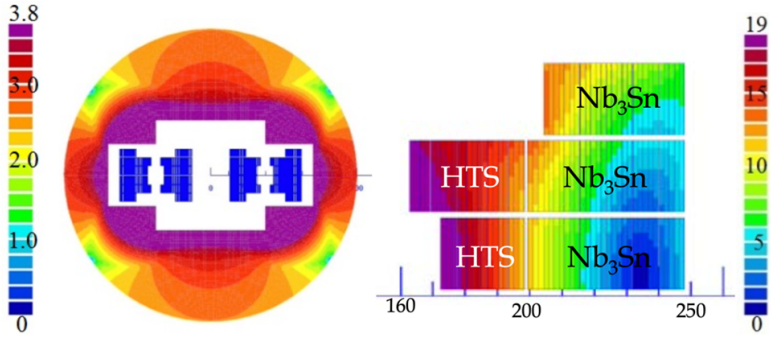

Fig. 6. Cross section of the 20 T block dipole designed in Ref. 22 based on two material grades only, twin aperture magnet (left) and one quarter of the coil (right).

assumptions in Ref. 22 is aimed at stress reduction and magnet protection margin, extrapolating from present engineering and applying conservative limits. The result is a modest current density, below 400 A/mm^2. This explains the relatively large coil cross section, and the value of the stored energy density in the coil being comparable to that of the 16 T Nb_3Sn dipole (as well as mechanical stress, not reported here). The design in Ref. 22 projected an outer diameter of the iron yoke of 800 mm. This should be increased to include the structural features necessary for the cold mass. Given the large level of electromagnetic force and the block structure, a bladder and key support and loading concept would be suitable, but would need the addition of a stiff shell around the iron yoke. Typical shell thickness would be around 60 to 70 mm, and integration of a cold mass of 950 mmm diameter in a cryostat with outer diameter of 1200 mm may pose challenges.

The relatively large coil area, driven by the modes current density, results in a significant cost increase. Even in the optimistic scenario of successful cost reduction, the projected cost of the 20 T dipole would be 1.5 times that of the HL-LHC reference (REBCO was assumed for the HTS material).

As for technology readiness, this is presently at the level of a conceptual study, and the TRL assigned is hence low, a value of 2 (technology concept formulated). Indeed, no such dipole has ever been built. Although it is thought to be possible to boost the field of an LTS outsert with an HTS insert, by building them separately and assembling them once completed, the electromagnetic and mechanical interaction of the two magnets is by no

means trivial. In addition to the development required for the LTS part, already listed in the section on the 16 T dipole, a suitable HTS insert technology should be validated beyond the initial results available at present.[42] Integration of the HTS insert in the LTS background implies that the hybrid dipole is designed as a whole, rather than two separate magnets. A good example of successful integration is provided by HTS/LTS UHF NMR solenoids[43] and solenoid magnets for high-field science.[44]

3.4. *24 T dipole*

The most ambitious design is the 24 T dipole of Ref. 19, a hybrid LTS/HTS built as an assembly of block coils, and shown schematically in Fig. 7. The outer low field grade coils, below 16 T, are made of Nb_3Sn, while the inner high field coils are made of Bi-2212. Besides the use of bladder and keys already described earlier, this 24 T dipole relies on stress management to deal with the spectacular increase of electromagnetic force. This is achieved by introducing structural supports within the blocks, whose purpose is to intercept part of the load and avoid accumulation. A second interesting feature is the use of a flux plate inserted between the lower and upper coils of a pole that provides means to compensate for persistent current effects at low field, i.e. injection conditions where the beam is most sensitive. Finally, in order to keep the outer diameter of the magnet small, small Nb-Ti windings are placed at the periphery of the iron yoke. These windings

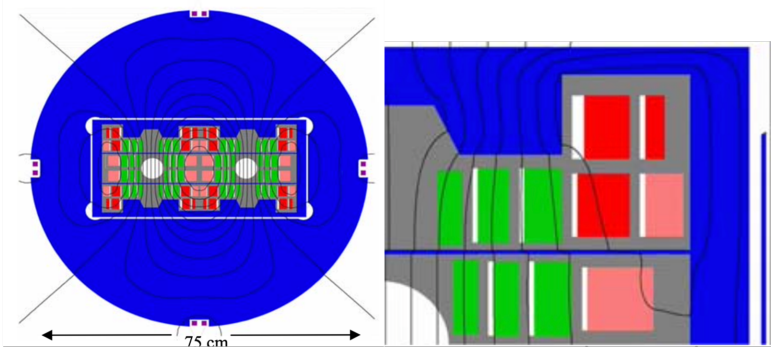

Fig. 7. Cross section of the 24 T LTS/HTS hybrid block dipole proposed in Ref. 19. Twin aperture assembly (left) showing Nb-Ti windings for flux cancellation at the outer diameter of the iron yoke, and one quarter coil cross section (right) showing the HTS (green) and LTS (red) grades, the stress management structure (grey) and the flux plate between lower and upper coils.

are powered to cancel the leaking flux and thus reduce stray field in the vicinity of the cold mass.

As we see from the summary values of Table 2, the coil cross section is kept very compact when compared to the 20 T dipole described above (note that we do not count the stress management structure in the coil cross section). This yields a relatively high current density, and stored energy density. While mechanical stress may be reduced and controlled thanks to stress management, the combination of high stored energy (large inductance), current density (fast heating rate in case of quench) and energy density (high hot-spot temperature) will pose a protection challenge. The cold mass diameter was designed in Ref. 19 using active magnetic shielding, and limited to an iron yoke diameter of 750 mm. Structural components are not considered in this diameter, but given the increase in outer dimension brought by active shielding, an integration into a 1200 mm cryostat seems possible.

Just as for the 20 T dipole, in this case the level of technology readiness is low, a value of 2 is assigned (technology concept formulated), and the issues to be resolved are essentially the same. Additional, in this case the projected cost is further driven up by the HTS material. Under our assumptions, and even with the projected cost reduction, a 24 T dipole built with Nb_3Sn and Bi-2212 would cost around the order of 5 times the HL-LHC reference. This is mainly driven by the contribution of Bi-2212. At such absolute cost, ranging in the several tens of MCHF for a 15 m long dipole, a HE41 would not be an interesting option.

4. Discussion

Beyond the technical feasibility of the designs presented above, it is interesting to look at the relative costs indicators to guide towards the most interesting long-term developments. Restricting ourselves to the hypotheses and studies reported, at first view only a 12 T and 16 T Nb_3Sn dipole magnet system would be at an affordable level, i.e. a unit cost below that of the HL-LHC Nb_3Sn magnets. The LTS/HTS hybrid options are presently out of a reasonable cost range. Even assuming a rather optimistic reduction of the superconductor cost, dipole magnet systems in the range of 20 T to 24 T are still nearly two to five times as expensive as the current HL-LHC Nb_3Sn magnet. The main reason is that the field generated by a dipole coil of given operating current density is proportional to the amount of conductor, hence to its mass and, in last instance, its cost. In addition,

the decrease of critical current density with field, the increased electromagnetic forces (scaling like B^2), and the increased stored energy (also scaling like B^2) tend to reduce the maximum allowable operating current density, further increasing the required amount of conductor and cost.

Given these simple considerations, there is only one way to reduce the cost of high field magnets — increasing their current density. This is in fact the first main asset of HTS materials, whose engineering critical current densities nowadays exceed 2000 A/mm^2 in the range of 20 T and at 4.2 K.[45] Besides, HTS magnets do not train, profiting from the large enthalpy reserve deriving from their high critical temperature (compared to LTS). It is hence not necessary to assume large operating margins with respect to the critical surface, as was assumed for LTS. Research is also on-going on how to make HTS winding solid and self-protecting, using a combination of structural and electrical ingenuity such as non-insulated (NI), metal-insulated (MI) or, more in general, controlled-insulation (CI) coils.[46] Such windings have no insulating layers, they are soldered, forming a solid mechanical component. Small demonstrators have shown that it is possible to exploit this technique to generate large solenoid fields, from 20 T to record values in excess of 45 T,[47] with winding current densities just short of 1000 A/mm^2. CI windings do not respond to ramps like a classical accelerator magnet, exhibiting field delays, drifts, and large remnant fields. It is nonetheless unquestionable that tapping on such potential for an increase of operating current density, by a good factor of two with respect to the assumptions taken for the design of the dipoles described earlier, would significantly change the perspective. A 16 T dipole built with CI HTS would be cheaper than an HL-LHC Nb_3Sn magnet, the 20 T dipole would have similar unit cost, and the 24 T dipole would be a factor of 1.3 more expensive, i.e. all in range of consideration for a HE-LHC.

The second main asset of HTS materials, especially driven by the recent developments for fusion application, is that they can operate at temperatures significantly higher than liquid helium. The range of 10 K to 20 K is of particular interest, because the loss in critical current density at high field at this temperature is limited (by a factor of two in the worst case of 20 K operation). In this range it is possible to devise cooling with gaseous helium, or other solutions such as *dry winding* with thermal links to a cold sink, e.g. a long pipe cooled by gas flow. The increased temperature would improve cryogenic efficiency, and reduce power consumption, by an estimated factor of two to four. At the same time the helium inventory would be reduced by a large amount, possibly up to an order of magnitude.

This would help mitigate the risks of helium availability and cost volatility, which are presently recognized as a definite concern for any future cryogenic installation, especially at the scale considered here.

Given these considerations on such large unexploited potential, it seems that development of HTS for the next step collider should be given high priority. This would offer magnet options to increase the LHC energy by two to three times, well beyond the reach of Nb_3Sn, but with a comparable projected cost, increased cryogenic efficiency, and reduced helium inventory.

5. Other Collider Challenges

In addition to the arc magnets, several other magnet systems will be required. Most important and most challenging are the sc final-focusing quadrupoles in the high-luminosity interaction regions, the sc separation dipoles, sc dipole magnets for the dispersion suppressors, and the (possibly warm) quadrupoles and dipoles in the collimation insertions.[4] The accelerator footprint must fit into the existing tunnel; see some pertinent discussions in Ref. 6. The collimation insertion itself poses several new challenges.[48]

An rf voltage of 16 MV is required per beam, the same value as for the present LHC. The rf power demand depends on the speed of acceleration. With a total stored beam energy of 4 GJ, a ramp duration of e.g. 30 minutes implies an rf power of at least 2 MW.

Crab cavities are needed to realize effective head-on collisions. Since the crossing angle decreases roughly as the inverse energy, the crab-cavity rf voltage, scaling as the product of crossing angle and beam energy, is similar to the HL-LHC's. However, crossing angle and required crab-cavity voltage also depend on the length of the final quadrupole triplet, which may grow with increasing beam energy. A novel Nb/Cu crab cavity consisting of a ridged waveguide resonator with wide-open apertures ("WOW")[49] could be an interesting option for the HE-LHC.

For the collider vacuum system, the rather voluminous beam screen developed for the FCC-hh,[50] which was successfully tested with FCC-hh like synchrotron radiation at a beamline in Karlsruhe,[51] provides excellent vacuum performance[52] and, by efficiently shielding the pumping slots, a low beam impedance.[53] In addition, suppression of electron-cloud build up may require either laser ablated surface engineering (LASE) treatment,[54] or amorphous carbon coating (a-C),[55] on parts of the inner beamscreen wall. An intriguing proposal is to coat either all or the remaining uncoated

portions of the inner beamscreen chamber with a thin layer ($\sim$1 μm) of high-temperature superconductor, to reduce the resistive-wall impedance.[56,57]

Injection into the HE-LHC at beam energies from 0.6 to 1.2 TeV requires a new sc SPS in the existing SPS tunnel. A conceptual design for such a machine with a top energy of 1.3 TeV was developed.[58] The higher beam energies also imply upgrades and technology developments for the injection system and for the beam dump; see e.g. Ref. 59.

Numerous other accelerator systems, such as cryogenics, electric distribution, cooling and ventilation, infrastructures for the experiments, etc., deserve consideration. The HE-LHC Conceptual Design Report[4] provides a comprehensive overview and helpful starting points for further development, as do the existing LHC systems.

6. Conclusions

In this chapter, building on past studies, we have explored how future high-field dipole magnets of various fields between 12 and 24 T, if (or when) they become available, could be used to construct a High-Energy Large Hadron Collider (HE-LHC) in the existing LHC tunnel. For each field and energy level, we discussed the collider performance that can be achieved, and looked at the corresponding magnet designs, their estimated technology readiness, and relative cost projection.

The main result of the analysis is that none of the HE-LHC options considered seems to come out as a true *sweet spot* for a higher energy LHC. An *affordable* but still costly 12 T dipole, which could be produced with technology at hand, would only yield a very modest centre-of-mass energy of 20 TeV. This is barely 50% above the present LHC, and the effort and resources necessary are hard to justify, while lacking a solid discovery perspective within this energy range. Any other option, and in particular pushing towards the high end of the dipole field, e.g., 24 T thanks to the use of HTS, would extend the energy reach by a good factor. At the same time, the scaling based on standard accelerator magnet technology would assign a price tag too excessive to these magnets to be considered for an energy upgrade at all, let alone the technology development required to reach this field level.

However, looking into the magnet cost drivers, we can see a major opportunity in the use of HTS. Adopting new magnet technology, i.e. compact winding with high current density thanks to specific features of HTS, may break standard scaling. This direction is similar to on-going work in other

domains of science and energy applications, and may produce the cost benefit required for a future application.

In fact, it is clear that the technology development outlined above would be beneficial not only for an energy upgrade of the LHC, but would also produce interesting alternatives to the baseline FCC-hh magnetic system, as well as the technology solutions sought for a muon collider. As we discussed briefly, compact HTS magnets could be significantly more energy efficient than an LTS magnet system, and reduce the long term risk of helium availability and cost, definite bonuses along the lines of sustainable science.

These considerations call for an increased effort towards HTS accelerator magnet R&D, seeking specifically conceptual designs and demonstration beyond present standards. Reaching this *technology hinge* may answer the question which, if any, of the various collider options, could, or should, be built and when.

Finally, for a higher energy hadron collider in the LHC tunnel, the beam parameters required at injection are already available today, and the beam dynamics at higher energy poses no particular challenges. A new feature compared to the present LHC is the much higher synchrotron radiation power. The resulting heat could be more efficiently removed if the arc magnets operate at a temperature higher than 1.9 K, which would be supported by HTS magnet technology. Another consequence of the enhanced synchrotron radiation is that the HE-LHC luminosity evolution during a physics fill will be determined by the combined effects of proton burn-off and significant radiation damping. Counteracting the latter, both longitudinal and transverse emittance blow up by controlled noise excitation are likely necessary to maintain longitudinal Landau damping and an acceptable beam-beam tune shift, respectively.

References

1. O. S. Brüning, R. Cappi, R. Garoby, O. Gröbner, W. Herr, T. P. R. Linnecar, R. Ostojic, K. Potter, L. Rossi, F. Ruggiero, K. Schindl, G. R. Stevenson, L. Tavian, T. Taylor, E. Tsesmelis, E. Weisse, F. Zimmermann, LHC Luminosity and Energy Upgrade: A Feasibility Study, Tech. rep., CERN, Geneva (Dec 2002). URL `http://cds.cern.ch/record/601847`
2. E. Todesco, F. Zimmermann (Eds.), EuCARD-AccNet-EuroLumi Workshop: The High-Energy Large Hadron Collider: Villa Bighi, Malta, Republic of Malta 14–16 Oct 2010, CERN, CERN, Geneva, 2011, 29 lectures, 156 pages, published as CERN Yellow Report. `doi:10.5170/CERN-2011-003`. URL `http://cds.cern.ch/record/1344820`

3. M. Benedikt, M. Capeans Garrido, F. Cerutti, B. Goddard, J. Gutleber, J.M. Jimenez, M. Mangano, V. Mertens, J.A. Osborne, T. Otto, K. Poole, W. Riegler, D. Schulte, L.J. Tavian, D. Tommasini, F. Zimmermann, FCC-hh: The Hadron Collider, Eur. Phys. J. Spec. Top. 228 (2019). URL https://doi.org/10.1140/epjst/e2019-900087-0
4. F. Zimmermann, M. Benedikt, M. Capeans Garrido, F. Cerutti, B. Goddard, J. Gutleber, J. M. Jimenez, M. Mangano, V. Mertens, J. A. Osborne, T. Otto, J. Poole, W. Riegler, L. J. Tavian, D. Tommasini, HE-LHC: The High-Energy Large Hadron Collider: Future Circular Collider Conceptual Design Report Volume 4. Future Circular Collider, The European Physical Journal Special Topics 228 (2019) 1109. doi:10.1140/epjst/e2019-900088-6. URL http://cds.cern.ch/record/2651305
5. Brüning, Oliver et al., LHC Full Energy Exploitation Study: Upgrade for Operation Beyond Ultimate Energy of 7.5 TeV, Tech. rep., CERN, Geneva (Sep 2020). URL https://cds.cern.ch/record/2729796
6. J. Keintzel et al., Lattice and optics options for possible energy upgrades of the Large Hadron Collider, Phys. Rev. Acc. Beams 23 (2020). URL https://journals.aps.org/prab/abstract/10.1103/PhysRevAccelBeams.23.101602
7. H. Damerau, A. Funken, R. Garoby, S. Gilardoni, B. Goddard, K. Hanke, A. Lombardi, D. Manglunki, M. Meddahi, B. Mikulec, G. Rumolo, E. Shaposhnikova, M. Vretenar, J. Coupard, LHC Injectors Upgrade, Technical Design Report, 2014. doi:10.17181/CERN.7NHR.6HGC. URL http://cds.cern.ch/record/1976692
8. E. N. Shaposhnikova, T. Argyropoulos, T. Bohl, C. M. Bhat, P. Baudrenghien, A. C. Butterworth, T. Mastoridis, J. Esteban Muller, G. Papotti, J. Tuckmantel, W. Venturini Delsolaro, U. Wehrle, Loss of Landau Damping in the LHC (2011) 3 p. URL http://cds.cern.ch/record/1378465
9. P. Baudrenghien, A. Butterworth, M. Jaussi, T. Mastoridis, G. Papotti, E. Shaposhnikova, J. Tuckmantel, Longitudinal emittance blow-up in the LHC (2011) 4 p. URL http://cds.cern.ch/record/1378464
10. G. Iadarola, HL-LHC filling schemes: possible optimization, 140th HiLumi WP2 Meeting, 29 January 2019.
11. M. Benedikt, D. Schulte, F. Zimmermann, Optimizing integrated luminosity of future hadron colliders, Phys. Rev. ST Accel. Beams 18 (2015) 101002. doi:10.1103/PhysRevSTAB.18.101002. URL https://link.aps.org/doi/10.1103/PhysRevSTAB.18.101002
12. C. O. Domínguez Sánchez de la Blanca, Electron cloud studies for the LHC and future proton colliders, PhD thesis, EPFL Lausanne (Jan 2014). URL http://cds.cern.ch/record/1645669
13. J. R. Cudell, V. V. Ezhela, P. Gauron, K. Kang, Y. V. Kuyanov, S. B. Lugovsky, E. Martynov, B. Nicolescu, E. A. Razuvaev, N. P. Tkachenko, Benchmarks for the forward observables at rhic, the tevatron-run ii, and the lhc, Phys. Rev. Lett. 89 (2002) 201801. doi:10.1103/PhysRevLett.89.201801. URL https://link.aps.org/doi/10.1103/PhysRevLett.89.201801

14. Latino, Giuseppe, Summary of physics results from the totem experiment, EPJ Web of Conferences 49 (2013) 02005. doi:10.1051/epjconf/20134902005. URL https://doi.org/10.1051/epjconf/20134902005
15. M. Menon, P. Silva, An updated analysis on the rise of the hadronic total cross-section at the lhc energy region, International Journal of Modern Physics A 28 (20) (2013) 1350099. arXiv:https://doi.org/10.1142/S0217751X13500991, doi:10.1142/S0217751X13500991.
URL https://doi.org/10.1142/S0217751X13500991
16. G. Antchev et al., Luminosity-independent measurements of total, elastic and inelastic cross-sections at $\sqrt{=}7$ TeV, EPL (Europhysics Letters) 101 (2) (2013) 21004. doi:10.1209/0295-5075/101/21004.
URL https://doi.org/10.1209/0295-5075/101/21004
17. G. Antchev et al., Luminosity-independent measurement of the proton-proton total cross section at $\sqrt{s} = 8$ TeV, Phys. Rev. Lett. 111 (2013) 012001. doi:10.1103/PhysRevLett.111.012001.
URL https://link.aps.org/doi/10.1103/PhysRevLett.111.012001
18. F. Bordry, M. Benedikt, O. Bruning, J. Jowett, L. Rossi, D. Schulte, S. Stapnes, F. Zimmermann, Machine Parameters and Projected Luminosity Performance of Proposed Future Colliders at CERN, Tech. rep., CERN, Geneva, * Temporary entry * (Oct 2018). arXiv:1810.13022.
URL http://cds.cern.ch/record/2645151
19. P. M. McIntyre, A. Sattarov, On the Feasibility of a Tripler Upgrade for LHC (2005). URL http://cds.cern.ch/record/926779
20. R. Assmann, R. Bailey, O. Brüning, O. Dominguez Sanchez, G. de Rijk, J. M. Jimenez, S. Myers, L. Rossi, L. Tavian, E. Todesco, F. Zimmermann, First Thoughts on a Higher-Energy LHC, Tech. rep., CERN, Geneva (Aug 2010). URL http://cds.cern.ch/record/1284326
21. L. Rossi, E. Todesco, Conceptual design of 20 T dipoles for high-energy LHC, arXiv 1108.1619 (Aug 2011). doi:10.5170/CERN-2011-003.13.
URL http://cds.cern.ch/record/1373969
22. E. Todesco, L. Bottura, G. De Rijk, L. Rossi, Dipoles for High-Energy LHC, IEEE Trans. Appl. Supercond. 24 (2014) 4004306. 6 p. doi:10.1109/TASC.2013.2286002. URL http://cds.cern.ch/record/1662724
23. D. Tommasini et al., Status of the 16 T Dipole Development Program for a Future Hadron Collider, IEEE Transactions on Applied Superconductivity 28 (2018) 4001305.
24. O. Aberle et al., High-Luminosity Large Hadron Collider (HL-LHC): Technical design report, CERN Yellow Reports: Monographs, CERN, Geneva, 2020. doi:10.23731/CYRM-2020-0010. URL http://cds.cern.ch/record/2749422
25. Alexander V. Zlobin, Nb_3Sn 11 T Dipole for the High Luminosity LHC (FNAL), in *Nb_3Sn Accelerator Magnets: Designs, Technologies and Performance* (eds. D. Schoerling and A.V. Zlobin), Springer International Publishing (2019) 193–222, doi:{10.1007/978-3-030-16118-7_8}.
26. Bernado Bordini et al., Nb_3Sn 11 T Dipole for the High Luminosity LHC (CERN), in *Nb_3Sn Accelerator Magnets: Designs, Technologies and Perfor-*

mance (eds. D. Schoerling and A.V. Zlobin), Springer International Publishing (2019) 223–258, doi:{10.1007/978-3-030-16118-7_9}.

27. A. Ballarino, L. Bottura, Targets for R&D on Nb_3Sn conductor for High Energy Physics, IEEE Trans. Appl. Supercond. 25 (2015) 6000906. 6 p. doi:10.1109/TASC.2015.2390149. URL http://cds.cern.ch/record/1987573
28. L. D. Cooley, A. K. Ghosh, R. M. Scanlan, Costs of high-field superconducting strands for particle accelerator magnets, Supercond. Sci. Technol. 18 (2005) R51–65. URL http://cds.cern.ch/record/909109
29. M. Karppinen et al., Design of 11 T twin-aperture Nb_3Sn dipole: Demonstrator magnet for LHC upgrades, IEEE Trans. Appl. Sup. 22 (3) (2012) 4901504. URL https://doi.org/10.1109/TASC.2011.2177625
30. A. Devred, Status of the 11 T dipole and CERN magnet programs beyond HiLumi, presented at the 9^{th} HL-LHC Collaboration Meeting, Fermilab, 14–16 Oct. 2019 (October 2019).
URL https://indico.cern.ch/event/806637/contributions/3487461/
31. C. Adolphsen et al., European Strategy for Particle Physics - Accelerator R&D Roadmap. European Strategy for Particle Physics – Accelerator R&D Roadmap, Vol. 1 of CERN Yellow Reports: Monographs, 2022. doi:10.23731/CYRM-2022-001. URL http://cds.cern.ch/record/2800190
32. P. Ferracin et al., Magnet design of the 150 mm aperture low-β quadrupoles for the High Luminosity LHC, IEEE Trans. Appl. Sup. 24 (3) (2013) 4002306. URL https://doi.org/10.1109/TASC.2013.2284970
33. D. Schoerling, A. Z. (eds.), Nb_3Sn accelerator magnets, Particle Acceleration and Detection Series, Springer, Cham, 2019.
URL https://doi.org/10.1007/978-3-030-16118-7
34. J. C. P. et al., 16 T Nb_3Sn racetrack model coil test result, IEEE Trans. Appl. Supercond. 26 (4) (2015) 4004906.
URL https://doi.org/10.1109/TASC.2016.2530684
35. C. News, A demonstrator magnet produces a record magnet field (March, 2020). URL https://home.cern/news/news/accelerators/demonstrator-magnet-produces-record-magnet-field
36. P. McIntyre, A. Sattarov, Nb_3Sn accelerator magnets, Particle Acceleration and Detection Series, Springer, Cham, 2019, Ch. Block-Type Nb_3Sn Dipole R&D at Texas A&M University.
URL https://doi.org/10.1007/978-3-030-16118-7_12
37. G. Sabbi, Nb_3Sn Accelerator Magnets. Particle Acceleration and Detection, Springer, 2019, Ch. The HD Block-Coil Dipole Program at LBNL, pp. 285–310.
38. E. Rochepault, P. Ferracin, Nb_3Sn accelerator magnets, Particle Acceleration and Detection Series, Springer, Cham, 2019, Ch. CEA–CERN block-type dipole magnet for cable testing: FRESCA2.
URL https://doi.org/10.1007/978-3-030-16118-7_12
39. I. P. et al., Cable design and development for the high-temperature superconductor cable test facility magnet, IEEE Trans. Appl. Supercond. 31 (7) (2021) 4804505. URL https://doi.org/10.1109/TASC.2021.3094410
40. J. L. R. Fernández, D. Arbelaez, P. Ferracin, R. Hafalia, R. Lee, P. Mallon,

S. Prestemon, G. Sabbi, T. Tristan, G. Vallone, Engineering design of a large aperture 15 t cable test facility dipole magnet, IEEE Transactions on Applied Superconductivity 32 (6) (2022) 1–5. doi:10.1109/TASC.2022.3158642.

41. S. Izquierdo-Bermudez, private communication (2017).
42. L. Rossi, C. Senatore, HTS accelerator magnet and conductor development in Europe, Instruments 5 (2021) 8. URL https://doi.org/10.3390/instruments5010008
43. Bruker Presse release, World's first 1.2 GHz high-resolution protein NMR data. URL http://cern.ch/go/Kn9F
44. H. Weijers et al., Progress in the development of a superconducting 32 t magnet with rebco high field coils, IEEE Transactions on Applied Superconductivity 24 (3) (2014) 4301805.
45. A. Molodyk et al., Development and large volume production of extremely high current density $YBa_2Cu_3O_7$ superconducting wires for fusion, Scientific Reports 11 (5) (2021) 2084.
URL https://doi.org/10.1038/s41598-021-81559-z
46. S. Hahn et al., Current Status of and Challenges for No-Insulation HTS Winding Technique, TEION KOGAKU (J. Soc. Jpn Cryo. Super) 53 (1) (2018) 2–9.
47. S. Hahn et al., 45.5-tesla direct-current magnetic field generated with a high-temperature superconducting magnet, Nature 570 (2019) 496–499.
48. M. Varasteh, R. Bruce, F. Cerutti, M. Crouch, F. Zimmermann, Impact of betatron collimation losses in the high-energy large hadron collider, Phys. Rev. Accel. Beams 24 (2021) 041601. doi:10.1103/PhysRevAccelBeams.24.041601.
URL https://link.aps.org/doi/10.1103/PhysRevAccelBeams.24.041601
49. K. Papke, A. Amorim Carvalho, C. Zanoni, A. Grudiev, Design studies of a compact superconducting RF crab cavity for future colliders using Nb/Cu technology (Jul 2019). URL http://cds.cern.ch/record/2683894
50. I. Bellafont, M. Morrone, L. Mether, J. Fernández, R. Kersevan, C. Garion, V. Baglin, P. Chiggiato, F. Pérez, Design of the future circular hadron collider beam vacuum chamber, Phys. Rev. Accel. Beams 23 (2020) 033201. doi:10.1103/PhysRevAccelBeams.23.033201.
URL https://link.aps.org/doi/10.1103/PhysRevAccelBeams.23.033201
51. L. A. Gonzalez, M. Gil-Costa, V. Baglin, P. Chiggiato, C. Garion, R. Kersevan, S. Casalbuoni, E. Huttel, I. Bellafont, F. Perez, Commissioning of a beam screen test bench experiment with a future circular hadron collider type synchrotron radiation beam, Phys. Rev. Accel. Beams 22 (2019) 083201. doi:10.1103/PhysRevAccelBeams.22.083201.
URL https://link.aps.org/doi/10.1103/PhysRevAccelBeams.22.083201
52. L. A. González, V. Baglin, P. Chiggiato, C. Garion, R. Kersevan, S. Casalbuoni, A. Grau, D. S. de Jauregui, I. Bellafont, F. Pérez, Photostimulated desorption performance of the future circular hadron collider beam screen, Phys. Rev. Accel. Beams 24 (2021) 113201. doi:10.1103/PhysRevAccelBeams.24.113201.
URL https://link.aps.org/doi/10.1103/PhysRevAccelBeams.24.113201

53. S. Arsenyev, D. Schulte, Broadband Impedance of Pumping Holes and Interconnects in the FCC-hh Beamscreen, J. Phys.: Conf. Ser. 1067 (2018) MOPMF030. 5 p. doi:10.18429/JACoW-IPAC2018-MOPMF030. URL http://cds.cern.ch/record/2647705
54. R. Valizadeh, O. B. Malyshev, S. Wang, S. A. Zolotovskaya, W. Allan Gillespie, A. Abdolvand, Low secondary electron yield engineered surface for electron cloud mitigation, Applied Physics Letters 105 (23) (2014) 231605. arXiv:https://doi.org/10.1063/1.4902993, doi:10.1063/1.4902993. URL https://doi.org/10.1063/1.4902993
55. C. Yin Vallgren, G. Arduini, J. Bauche, S. Calatroni, P. Chiggiato, K. Cornelis, P. C. Pinto, B. Henrist, E. Métral, H. Neupert, G. Rumolo, E. Shaposhnikova, M. Taborelli, Amorphous carbon coatings for the mitigation of electron cloud in the cern super proton synchrotron, Phys. Rev. ST Accel. Beams 14 (2011) 071001. doi:10.1103/PhysRevSTAB.14.071001. URL https://link.aps.org/doi/10.1103/PhysRevSTAB.14.071001
56. S. Calatroni, E. Bellingeri, C. Ferdeghini, M. Putti, R. Vaglio, T. Baumgartner, M. Eisterer, Thallium-based high-temperature superconductors for beam impedance mitigation in the future circular collider, Superconductor Science and Technology 30 (7) (2017) 075002. doi:10.1088/1361-6668/aa6bd0. URL https://doi.org/10.1088/1361-6668/aa6bd0
57. S. Calatroni, R. Vaglio, High-Temperature Superconductor Coatings for Beam Impedance Reduction in Particle Colliders: Nonlinear Effects, IEEE Trans. Appl. Supercond. 31 (2021) 3500208. 8 p. doi:10.1109/tasc.2021.3053299. URL http://cds.cern.ch/record/2776595
58. F. Burkart, W. Bartmann, M. Benedikt, B. Goddard, A. Milanese, J. Schmidt, Conceptual Design Considerations for a 1.3 TeV Superconducting SPS (scSPS) (2017) WEPVA033. 4 p doi:10.18429/JACoW-IPAC2017-WEPVA033. URL http://cds.cern.ch/record/2289465
59. W. Bartmann et al., Injection and Dump Systems for a 13.5 TeV Hadron Synchrotron HE-LHC, J. Phys. Conf. Ser. 1067 (5) (2018) 052021. doi:10.18429/JACoW-IPAC2018-TUPAF060.